1-1-2012

Low Coherence Interferometry Modelling using Combined Broadband Gaussian Light Sources

Paul Jansz

Graham Wild
Edith Cowan University

Steven Richardson
Edith Cowan University, s.richardson@ecu.edu.au

Steven Hinckley
Edith Cowan University, s.hinckley@ecu.edu.au

10.1117/12.916030

Low Coherence Interferometry Modelling using Combined Broadband Gaussian Light Sources

Paul Jansz, Graham Wild, Steven Richardson, and Steven Hinckley
School of Engineering, Edith Cowan University, 270 Joondalup Drive,
Joondalup, WA 6027, Australia
p.jansz@ecu.edu.au

ABSTRACT

Using a Low Coherence Interferometry (LCI) model, a comparison of broadband single-Gaussian and multi-Gaussian light sources has been undertaken. For single-Gaussian sources, the axial resolution improved with source bandwidth, confirming the coherence length relation that resolution for single Gaussian sources improves with increasing spectral bandwidth. However, narrow bandwidth light sources resulted in interferograms with overlapping strata peaks and the loss of individual strata information. For multiple-Gaussian sources with the same bandwidth, spectral side lobes increased, reducing A-scan reliability to show accurate layer information without eliminating the side lobes. The simulations show the conditions needed for resolution of strata information for broadband light sources using both single and multiple Gaussian models. The potential to use the model to study LCI and OCT light sources, optical delays and sample structures can better characterise these LCI and OCT elements. Forecasting misinformation in the interferogram, may allow preliminary corrections. With improvements to the LCI-OCT model, more applications are envisaged.

Keywords: Gaussian light source, Modelling, Optical Coherence Tomography, Medical Imaging.

1. INTRODUCTION

Optical Coherence Tomography (OCT) is an application subset of Low Coherence Interferometry (LCI). In LCI and OCT a low coherent/broadband near infrared source is used to generate a reflection intensity map of a material's (LCI) or tissue's (OCT) cross section, having 1 – 3 mm penetration depth [1] depending on tissue type and wavelength, and 1 – 10 μm axial resolution depending on the bandwidth, central wavelength [2] and the light source spectral shape [3].

In previous research [4] an OCT model was used to compare different optical delay lines (ODL) in order to verify the functionality of a proposed stationary ODL [5]. To further investigated OCT operation characteristics, the OCT model has been used to characterize one to four combined Gaussian broadband light sources which mimic the spectral characteristic of Super Luminescent Diodes (SLDs), a typical OCT light source.

The optical source's suitability is governed by its bandwidth, optical power, spectral shape, ripple, and cost. Figure 1, self generated in excel, and based on [2], shows the relationship between FWHM bandwidth ($\Delta\lambda$), central wavelength (λ_0) and coherence length (L_C). The wider the bandwidth, the better the axial resolution (R_{axial}) according to the coherence length (L_C) relation divided by the average tissue refractive index (n_{ave}):

$$R_{axial} = \frac{L_C}{n_{ave}} = \frac{\lambda_0^{\,2}.\ln(4)}{\pi.\Delta\lambda.n_{ave}} \tag{1}$$

The shape of the coherence function and the level of the side lobes are determined by the spectral shape. The inverse Fourier Transform of a Gaussian is itself Gaussian. Such a spectrum has no side lobes in the autocorrelation function, and as such it is the preferred source spectrum. Due to their affordability and Gaussian spectra, OCT sources are typically Super Luminescent Diodes (SLDs). To increase the bandwidth, so that axial resolution is improved, it is common to combine two or more SLDs. This often leads to non-Gaussian spectra with multiple spectral peaks degrading the A-scan with the addition of the spurious smaller "side lobe" peaks [6].

SLDs work like a forward biased PN junction, without feedback to prevent lasing, where a large forward bias creates a large density of recombining electrons and holes, resulting in light emission. Spontaneous emission is amplified due to

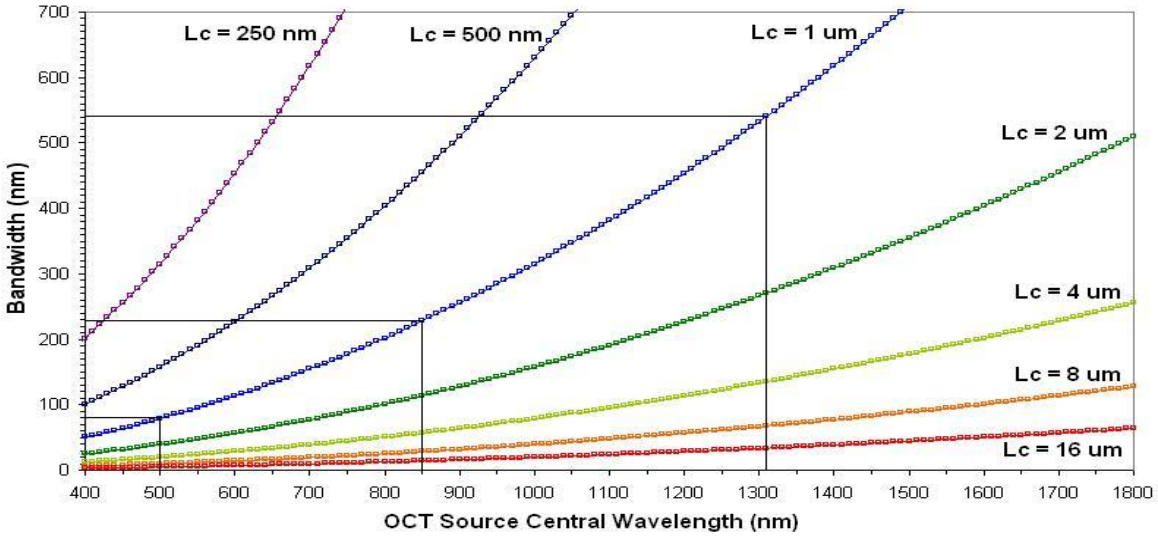

Figure 1. Free space OCT iso-resolution lines (iso-L_C lines); bandwidths for typical OCT sources (based on fig.8.2 [2])

high injection current, resulting in super-luminescence [7]. The current needs to be kept at a maximum value at which super-luminescence, not lasing, is generated [8]. The narrow emission angle of SLDs allows optimum coupling into single-mode fibre for optical fibre based OCT [9]. SLDs can be manufactured to illuminate within and beyond the "therapeutic window". This spectral "window" is between 800 and 1350 nm [7].

The first SLDs were based on bulk semiconductor hetero-structures with thick active layers. Their optical spectrum width varied from 15 – 20 nm for 800 nm AlGaAs emitters to 30 – 40 nm for 1300 – 1550 nm InGaAsP SLDs. Broadening the spectrum was attempted for these bulk active layer SLDs by including a "stacked-layer-SLD" with two active layers of different material [3]. The most significant progress in spectral broadening was made with the demonstration of quantum-well SLDs. Their spectral broadening can be achieved in two ways. First, the optical gain of these SLDs is broadened by their higher density of states, compared to bulk SLDs. Secondly, transition from different sub-bands in quantum-well active layers, can be used to broaden the SLD spectrum [3]. This broadening is dependent on drive current, however as broadening increases the spectrum can become bi-lobed [10], resulting in expected spurious side lobes appearing in the interferogram, as mentioned previously.

Another method to increase bandwidth is to construct tandem SLDs with central wavelengths distributed sufficiently so that the spectra overlap. This can be achieved by physically connecting multiple SLDs with their outputs coupled optically. An early example of connecting SLDs, has two SLDs at 830nm (26nm bandwidth) and 855nm (25nm bandwidth), optically combined with a beam splitting cube. This resulted in a reduction of coherence length from 12μm to 8μm [11].

Wang [12] show another multi-SLD example. It is a combination of four SLDs with wavelengths-(bandwidth) (nm) being 1265-(30), 1320-(70), 1355-(53), and 1380-(47), respectively. The combined bandwidth produced was 145nm centred at 1330nm having an output of 10mW and coherence length of 5.4μm.

Other novel multi-SLD sources are the BroadLighter D-890 (2 SLDs), Q-940 and Q-1350 (4 SLDs) with bandwidth of 150nm, 300nm and 280nm, respectively [13]. An example of a quantum-well double SLD is the DenseLight DL-BD9-CS31159A, a 25mW SLD with a bandwidth of 170nm at 1310nm, and with L_C of 4.4μm [14].

This research considers the latter spectral broadening techniques. It compares the effect of combining multiple broadband Gaussian sources on their total spectrum, as well as characterizing the effect this has on the resultant interferogram, and the corresponding limitations for practical implementations. Importantly, this is for the same sample layer structure, enabling direct comparison. Multiple SLD bandwidth broadening is not the only broadening technique. While others present broader spectrums, multiple spectral peaks typically occur. This initial investigation demonstrates the relation between bandwidth ($\Delta\lambda$) and axial resolution (R_{axial}) for a given central wavelength (λ_0). It further compares the effect of bandwidth on the spectrum and autocorrelation function for combined Gaussian sources, corroborating current knowledge, as well as demonstrating the effect of bandwidth and the number of Gaussian sources used.

2. THEORY

2.1 Light Source:

The Light source is modelled as a spectrum of continuous wavelengths, with a Gaussian spectral shape defined by the peak amplitude (A_0), the peak wavelength (λ_0), and the spectral bandwidth, FWHM ($\Delta\lambda$), as:

$$A(\lambda) = A_0 Exp\left(\frac{-\ln(16)(\lambda - \lambda_0)^2}{(\Delta\lambda)^2} \right) \tag{2}$$

2.2 Light in Interferometer:

In the interferometer, light is split by a beam splitter; 50% is reflected (R) to the ODL and 50% is transmitted (T) to the sample. The light Amplitude after the split is:

$$A_R(\lambda) = A_T(\lambda) = \frac{A(\lambda)}{\sqrt{2}} \tag{3}$$

The Amplitudes after reflection from the sample interfaces are given by,

$$A_T(\lambda)_i = \frac{A(\lambda)}{\sqrt{2}} \sqrt{r_i} \prod_{j=1}^{i-1} (1 - r_j) \tag{4}$$

Here, $i = 1,\ldots,n$ is the index over the sample's semi-reflector interfaces, and r_i denotes the reflectivity of the i^{th} interface. The total distance from the laser source to the i^{th} reflecting sample interface and then back to the detector is denoted d_i. The model does not consider multiple reflections, considered to be negligible, due to the small reflection coefficients.

The ODL is a moving reference reflector, assumed to be moving slow enough to neglect the Doppler Effect. The distance from the laser source to the ODL reflector and back to the beam-splitter and then to the detector is denoted d_{n+1}. If the ODL Reflector moves an amount Δd, then d_{n+1} increases by an amount $2\Delta d$.

2.3 Light at Detector – Wave Interference:

The square of the Amplitude of the auto-correlated wave is:

$$[\text{Amplitude}(\lambda)]^2 = \frac{A(\lambda)^2}{4} \left[\left(\sum_{i=1}^{n+1} RF_i \cos\theta_i \right)^2 + \left(\sum_{i=1}^{n+1} RF_i \sin\theta_i \right)^2 \right] \tag{5}$$

where,

$$RF_i = \begin{cases} r_i \prod_{j=1}^{i-1} (1 - r_j), & i = 1,\ldots,n \\ 1, & i = n+1 \end{cases} \tag{6}$$

and,

$$\theta_i = \begin{cases} \frac{2\pi d_i}{\lambda} + \pi, & n_i < n_{i+1} \\ \frac{2\pi d_i}{\lambda}, & n_i > n_{i+1} \text{ or } i = n+1 \end{cases} \tag{7}$$

Therefore, the total intensity is:

$$\text{Total Intensity}(d_{n+1}) = \int_{-\infty}^{\infty} [\text{Amplitude}(\lambda)]^2 \, d\lambda \tag{8}$$

The integral in Equation (8) is approximated numerically.

3. RESULTS AND DISCUSSION

3.1 Single Source Varying Bandwidth

The layered virtual sample employed in the simulation consisted of five layers of equal thickness, being 100µm and 95µm in section 3.1 and 3.2, respectively. This thickness is analogous to tissue lamina *in-vivo* [15]. The refractive index assigned to the medium above the uppermost stratum was 1.35. The assigned refractive indices of the five sample layers, uppermost layer first, were 1.45, 1.49, 1.45, 1.49 and 1.45, respectively. Even though these values are within biological tissue ranges, 1.37 – 1.5 [15], the model may be used to explore any virtual multi-strata reflecting material.

The flexibility of this version (3.0) of the OCT simulation model to allow, at this stage, choice of two sample layer characteristics – thickness and refractive index – enables approximate definition of real axial tissue characteristics. This then generates an autocorrelation function with double the layer separation. For a user defined light source spectrum and optical delay line (ODL), the effects of OCT sources, ODLs [4] and sample types on OCT operation, can be studied.

Figure 2 shows the effect of Gaussian source bandwidth on layer resolution. As bandwidth increases, resolution increases. Note that side lobes are absent from the interferograms in Figure 2(b), (c) and (d). Layer resolution is not possible in Figure 2(a) because the L_C is 106µm and the layer thickness is only 100µm, which is $0.94L_C$. In contrast, the broadest source has best resolution because the L_C is ten times less for the same 100µm interface separation, which is $9.4L_C$. Even with (b) and (c), the layers can be resolved, their separations being $1.9L_C$ and $4.7L_C$, respectively. The hidden peak information in Figure 2(a) can lead to loss of layer information in the A-scans.

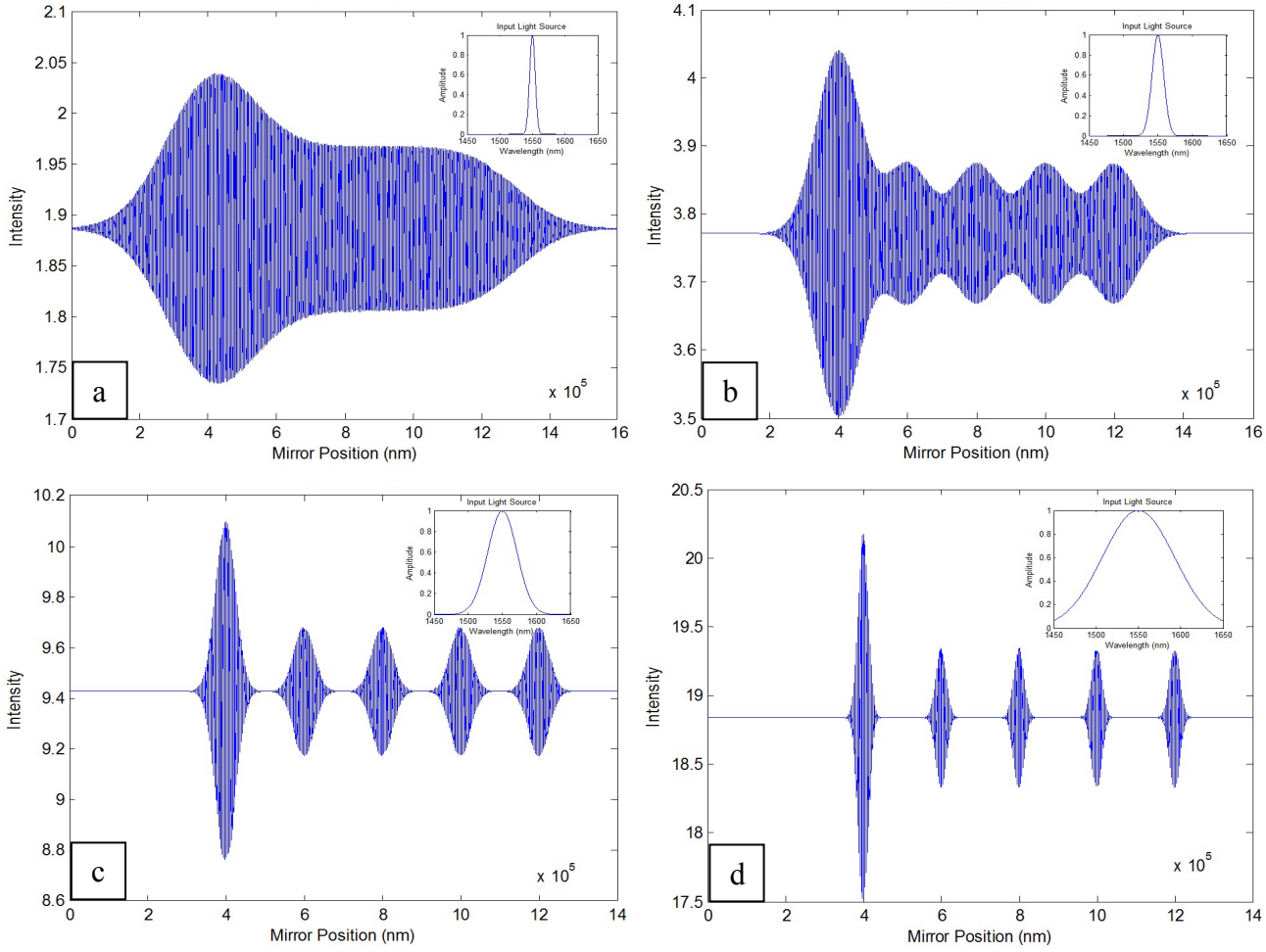

Figure 2. OCT Interferogram of a 5, 100µm thick layer virtual sample with the associated source spectrum insert. Source bandwidths are (a) 10 nm, (b) 20nm, (c) 50nm, and (d) 100nm, with central source wavelength of 1550nm.

3.2 Multiple Source with Constant Bandwidth

Figures 3, 4 and 5 show the interferograms for two, three and four combined Gaussian sources, respectively. Spurious side lobes now appear. Theoretically, if resolution is a function of the coherence length, then Figures 3, 4 and 5 should be as equally resolvable as Figure 2(d), as they have the same coherence lengths (10.6μm). This is, of course, not the case, as the non-Gaussian sources generate the classic side lobe artefact. The greater the peak separation in the spectrum, the greater the number of side lobes and their daughter satellites. There is one to two generations of side lobes for two combined sources (Figure 3), two to three for three combined sources (Figure 4) and three to four for four sources (Figure 5); also, the larger the reflection, the larger the side lobe and satellite magnitudes.

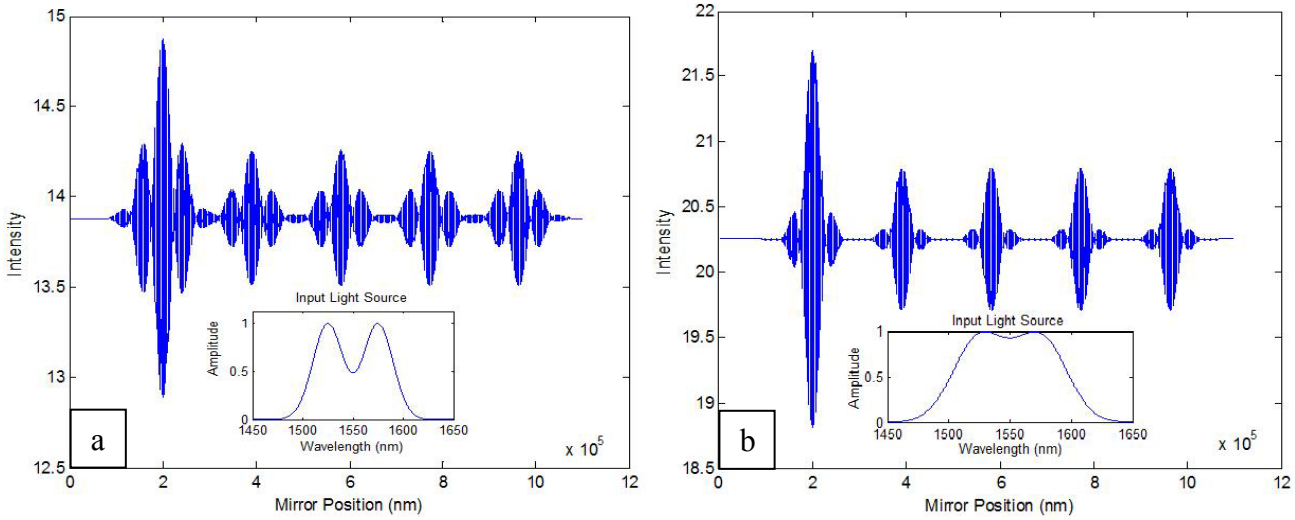

Figure 3. OCT Interferogram of 5, 95μm thick layer virtual sample with the associated 2 Gaussian source spectrum insert. The sources bandwidth (Δλ) / peak amplitude (Amax) / λ_0s are for (a) 35nm / 0.9965au / 1525,1575nm, and (b) 50nm / 0.9266au / 1525,1575nm.

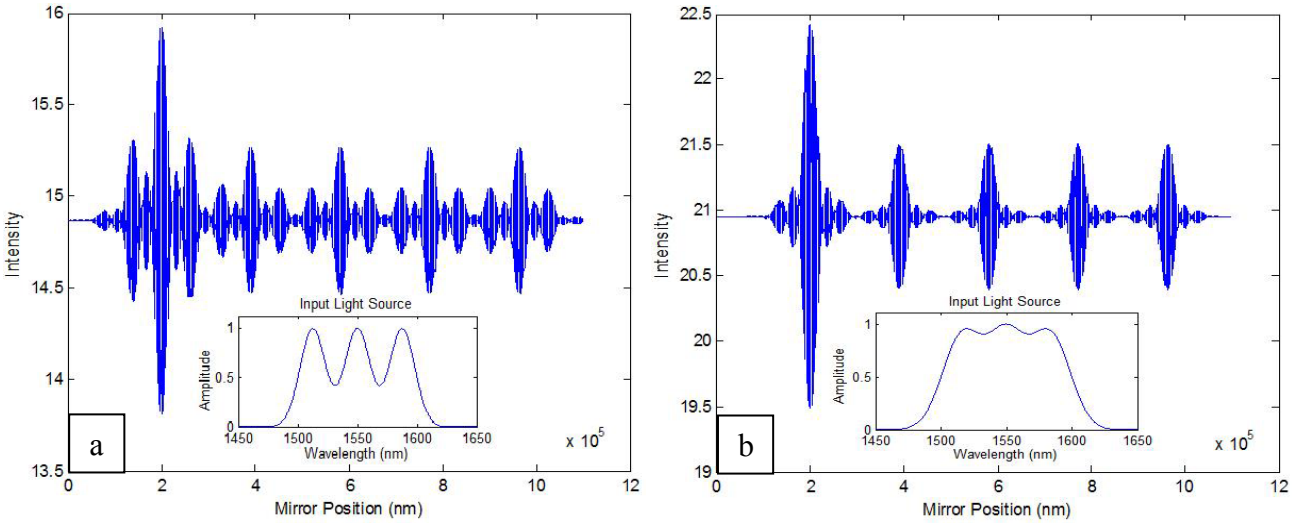

Figure 4. OCT Interferogram of 5, 95μm thick layer virtual sample with the associated 3 Gaussian source spectrum insert. The sources Δλ / A_{max} / λ_0s are for (a) 25nm / 0.9965au / 1512.5, 1550, 1587.5nm, and (b) 35nm / 0.8756au / 1516, 1550, 1584nm.

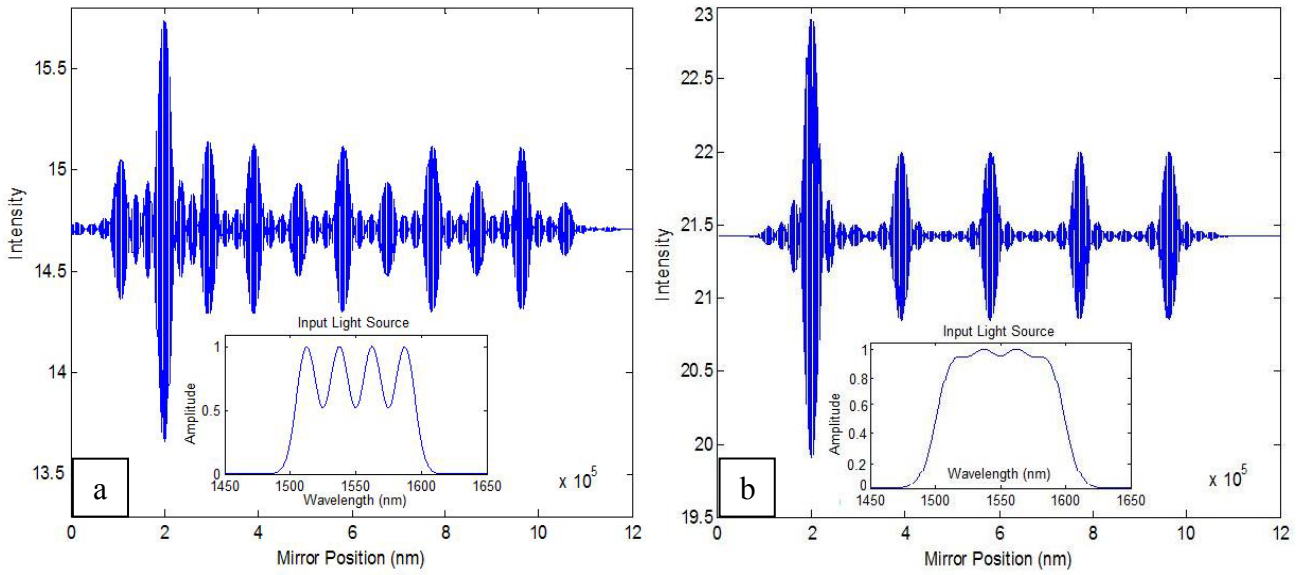

Figure 5. OCT Interferogram of 5, 95μm thick layer virtual sample with the associated 4 Gaussian source spectrum insert. The sources $\Delta\lambda$ / A_{max} / λ_0s are for (a) 18nm / 0.9908au / 1512.5, 1537.5, 1562.5, 1587.5nm, and (b) 28nm / 0.82au / 1512.5, 1537.5, 1562.5, 1587.5nm.

These complex interferogram results indicate that the side lobes would interact with each other to a greater extent as the layers narrow below $9L_c$. The result of this is that the phantom layers would appear as strong as the real layers. For example, in Figure 3(a), if the corresponding secondary peaks of two strata were to be in phase, and collocated, then the sum of this would be equal in magnitude to the primary peak. This phantom layer would appear to be located exactly between the two strata. The complex interaction is also seen in Figure 5(a), where the secondary peak of the front surface is identical to the main peak of the other layers. The result for the multiple layers shows that this effect is reduced as the separation between the sources is lessened.

Future research with this simulation model will explore (i) varying the strata thicknesses and its effect on the interferograms, and (ii) the effect of real OCT light source spectra on their interferogram characteristics. Already the MatLab model's simulation software has presented fresh insights from its capability to generate interferogram "movies". In particular, it can capture a sequence of interferograms as the layer thickness is stepwise increased or decreased, showing the change in layer peak and, where relevant, side lobe peak magnitude and morphology.

The current version of the OCT model is one dimensional. It considers ballistic sample reflections dependent on refractive index and interface separation. The potential to improve the model to study real OCT light sources by generating their auto-correlation functions for realistic samples, that considers additional tissue characteristics such as, absorption, scattering, dispersion and polarization, is envisaged. This will provide a more realistic understanding of OCT light source functionality for specific tissue types and conditions.

Due to the ongoing extrinsic evolution – i.e. the development of any non-autonomous, passive product or concept, over time, imposed upon the product or concept extrinsically [16] – of the OCT simulation software, more applications are envisaged. It will be able to forecast misinformation, for which corrections may be able to be made. It may also be able to provide insight into choosing the best real OCT light source for a given tissue application. Studying the effect of varying layer thickness on the interferogram may help in the understanding of new OCT modalities. Its use in physics, biomedical optics, imaging, and photonics education may also be possible.

4. CONCLUSION

We have shown a comparison of broadband single-Gaussian and multi-Gaussian light sources used for Optical Coherence Tomography (OCT). For single-Gaussian sources, the axial resolution improved with source bandwidth, as expected. However, for narrow bandwidth light sources, their interferograms showed overlapping strata peaks. This resulted in the loss of individual strata information. For an increasing number of multiple-Gaussian sources with the same bandwidth, spectral side lobes increased, reducing the reliability of the A-scan to show accurate layer information without eliminating the side lobes. The more Gaussian the light spectrum the more ideal the autocorrelation function. The potential to use the model to study real OCT light sources, optical delays and sample structures can improve our understanding of these OCT elements. With ongoing model development, more applications are envisaged.

REFERENCES

[1] Friebel, M., Helfmann, J., Netz, U., Meinke, M. "Influence of oxygen saturation on the optical scattering properties of human red blood cells in the spectral range 250 to 2000 nm", Journal of Biomedical Optics, 14(3), 034001-1 – 6 (2009).

[2] Drexler, W., Chen, Y., Aguirre, A., Povazay, B., Unterhuber, A., Fujimoto, J.G., "Ultrahigh resolution optical coherence tomography" in *Optical Coherence Tomography: Technology and Applications*, Drexler, W. and Fugimoto, J.G., Eds. Berlin, Springer-Verlag p239-79 (2008).

[3] Shidlovski, V.R., "Superluminescent diode light sources for OCT" in *Optical Coherence Tomography: Technology and Applications*, Drexler, W. and Fugimoto, J.G., Eds. Berlin, Springer-Verlag p281 - 99 (2008).

[4] Jansz, P.V., Wild, G., Richardson, S., Hinckley, S., "Simulation of optical delay lines for optical coherence tomography", Proc. IQEC-CLEO Pacific Rim, Sydney (2011).

[5] Jansz, P.V., Wild, G., Hinckley, S., "A micro-photonic stationary optical delay line for fibre optic TD OCT", Proc. OECC ACOFT (2008).

[6] Adie, S.G., "Enhancement of Contrast in Optical Coherence Tomography: New Modes, Methods and Technologies". PhD thesis, School of Electrical and Electronic Engineering, The University of Western Australia. (2007).

[7] Fercher, A.F., Drexler, W., Hitzenberger, C.K., Lasser, T., "Optical coherence tomography – principles and applications", Report on Progress in Physics, 66, 239 – 303 (2003).

[8] Zvyagin, A.V., Garcia-Webb, M. G., Sampson, D.D., "Semiconductor line source for low-coherence interferometry", Applied Optics, 40(6), 913 – 5, Feb 20 (2001).

[9] Parker, J.R., "Optical coherence tomography: Endoscopic Instrumentation and applications" (2003). Retrieved November 23, 2005, from the Imperial College website: http://www.imperial.ac.uk/research/photonics/about/staff/james_parker_octreport.pdf

[10] Rossetti, M., Markus, A., Fiore, A., Occhi, L., Velez, C., "Quantum dot superluminescent diodes emitting at 1.3μm", IEEE Photonics Technology Letters, 17(3), 540 – 2 (2005).

[11] Baumgartner, A., Hitzenberger, C.K., Ergun, E., Stur, M., Sattmann, H., Drexler, W., Fercher, A. F., "Resolution-improved dual-beam and standard optical coherence tomography: a comparison", Graefe's Arch. Clin. Exp. Ophthalmology, 238, 385 – 92 (2000).

[12] Wang, H., Jenkins, M.W., Rollins, A.M., "A combined multiple-SLED broadband light source at 1300 nm for high resolution optical coherence tomography", Optics Communications, 281(7), 1896-1900 (2008).

[13] Andreeva, E.V., Lapin, P.I., Prokhorov, V.V., Shidlovski, V.R., Shramenko, M.V., Yakubovich, S.D., "Novel superluminescent diodes and SLD-based light sources for optical coherence tomography". Proceedings of SPIE - OSA Biomedical Optics, 6627, 662703 -1 – 10 (2007).

[14] Lee, S., Jeong, H., Kim, B., "High-speed spectral domain polarization-sensitive optical coherence tomography using a single camera and an optical switch at 1.3μm". J. of Biomedical Optics, 15(1), 010501-1 – 3(2010).

[15] Van Gemert, M. J.C., Jacques S.L., Sterenborg, H.J.C.M., Star, W.M., "Skin optics". IEEE Trans. on Biomedical Engineering, 36(12), 1146 – 1154 (1989).

[16] Jansz, P.V., Hinckley, S., "Extrinsic Evolution of the Stacked Gradient Poly-Homojunction Photodiode Genre" in Advances in Photodiodes. Intech Publications. Croatia. Edit Gian-Franco Dalla Betta. pp 181 – 204. (2011)